Microfluidics

DOI: 10.1002/anie.200604112

# Fluorescence-Lifetime Imaging of DNA–Dye Interactions within Continuous-Flow Microfluidic Systems**

*Richard K. P. Benninger, Oliver Hofmann, Björn Önfelt, Ian Munro, Chris Dunsby, Daniel M. Davis, Mark A. A. Neil, Paul M. W. French,* and Andrew J. de Mello**

Recent years have seen significant progress in the development of microfabricated systems for use in the chemical and biological sciences.[1] Much of this development has been driven by a need to perform rapid measurements on small sample volumes in areas such as chemical synthesis,[2] DNA analysis,[3] drug discovery,[4] pharmaceutical screening,[5] proteomics,[6] and medical diagnostics.[7] It is well recognized that, when compared to macroscale instruments, microfluidic systems engender a number of distinct advantages with respect to speed, analytical throughput, reagent usage, process control, automation, and operational and configurational flexibility. Although all these advantages are directly facilitated by system downscaling (and the associated improvements in both mass and thermal transfer), the instantaneous-reaction volumes that characterize microfluidic systems typically range from a few picoliters to hundreds of nanoliters. This means that analyte detection and identification is a significant challenge and often defines the principal limitations of a microfluidic system.[8] Despite this problem, a variety of detection methods have been successfully transferred and integrated with microfluidic systems.[2]

[*] Dr. R. K. P. Benninger, I. Munro, Dr. C. Dunsby, Dr. M. A. A. Neil, Prof. P. M. W. French
Department of Physics
Imperial College London
Exhibition Road, South Kensington, London, SW72AZ (UK)
Fax: (+44) 207-594-7714
E-mail: paul.french@imperial.ac.uk
Dr. O. Hofmann, Prof. A. J. de Mello
Department of Chemistry
Imperial College London
Exhibition Road, South Kensington, London, SW72AZ (UK)
Fax: (+44) 207-594-5834
E-mail: a.demello@imperial.ac.uk
Dr. B. Önfelt, Prof. D. M. Davis
Department of Biological Sciences
Imperial College London
Exhibition Road, South Kensington, London, SW72AZ (UK)

[**] The authors acknowledge financial support from a Department of Trade and Industry Beacon award, the European Community (Framework VI Integrated Project "Integrated technologies for in vivo molecular imaging" contract number LSHG-CT-2003-503259), the Engineering and Physical Sciences Research Council (EPSRC), and Molecular Vision Ltd. R.K.P.B. acknowledges the award of a CASE studentship from the EPSRC and Kentech Instruments. B.Ö. acknowledges the award of a fellowship from the Wenner–Gren foundation.

Supporting information for this article is available on the WWW under http://www.angewandte.org or from the author.

The use of fluorescence as a readout mechanism in microfluidic systems is advantageous because of the high sensitivity, noninvasiveness, and ease of implementation of this method. Accordingly, fluorescence methods are routinely used in a wide range of analyses in single-point or imaging modalities. Although useful and easy to implement, steady-state (time-integrated) fluorescence methods are limited with respect to quantitative analysis of fluidic samples because of their sensitivity to experimental parameters such as optical pathlength, radiation scattering, inhomogeneous excitation, and fluorophore bleaching.[9] In contrast, time-resolved fluorescence techniques are particularly advantageous for quantifying fluorescence emission because their ratiometric nature makes them largely independent of instrumentation-based artifacts associated with excitation and detection efficiencies, background scattered radiation, and autofluorescence. The enhanced quantification available with fluorescence-lifetime imaging (FLIM) has recently been used by Benninger et al. to quantitatively map fluidic temperatures in microfluidic environments with micrometer spatial resolution.[10] Furthermore, FLIM has been used to perform three-dimensional spatial mapping of solvent viscosity and mixing[11] and to evaluate laminar flow in microfluidic systems.[12]

Herein we extend the utility of time-resolved fluorescence imaging as a detection modality for microfluidic systems by reporting the study of DNA–dye binding interactions in continuous-flow microfluidic reactors. In contrast to typical bulk studies of DNA–dye interactions where only the end point of a reaction is accessible,[13] the use of a continuous-flow microfluidic reactor enables the extraction of kinetic information through a time-to-space conversion, that is, multiple time points can be accessed by measuring at different positions along the mixing channel. Microfluidic systems therefore provide an ideal platform for studying the temporal variation in fluorescence kinetics during and after DNA–dye binding, while the application of time- and polarization-resolved fluorescence imaging facilitates the resolution of multiple reaction species through their respective decay kinetics and rotational mobility. Crucially, the combination of microfluidics and FLIM generates novel information that cannot be extracted from bulk measurements or time-integrated fluorescence signals alone. Specifically, in this study we demonstrate the resolution of emitting states of the DNA-intercalating dye Hoechst 33258 (H33258) as it binds to large DNA plasmids in the nonequilibrium conditions provided by a simple microfluidic reactor.

Time-resolved fluorescence imaging of the microfluidic environment was achieved by using a quasi-widefield multi-

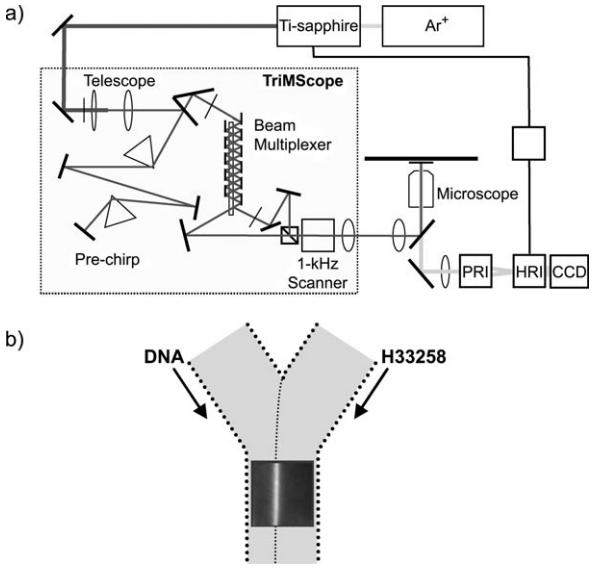


***Figure 1.*** a) Schematic representation of the 3D FLIM system: pulsed infrared illumination is coupled into the TriMScope for beam multiplexing and scanning. This illumination is focused onto the sample, where two-photon excitation occurs in only a thin optical section. The fluorescence emission is imaged onto a HRI read out by a CCD camera. For polarization resolution, the PRI is included in the detection path. b) Simplified representation of the microfluidic reactor.

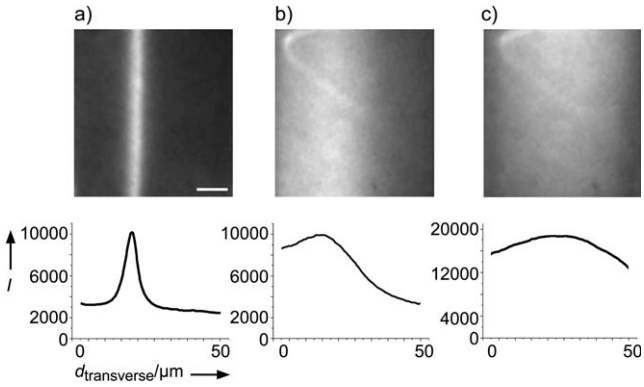


***Figure 2.*** DNA stream enters the mixing channel from the left-hand side, with the H33258 flow entering from the right. Representative time-integrated fluorescence-intensity images and cross-sectional profiles at different residence times from the point of confluence are shown: a) $t = 300$ ms, b) $t = 7.2$ s, c) imaged after zero flow for 10 min, that is, $t \rightarrow \infty$. The scale bar represents 10 μm. Increased fluorescence intensity is observed at the region of interdiffusion between the two flows, as H33258 binds to DNA. The asymmetric intensity profile across the channel in (b) reflects the fact that the smaller H33258 fluorophores diffuse more rapidly than the large DNA plasmids. In (a), the flow interface is to the left of center due to the 2:1 flow-rate ratio between the H33258 (right) and DNA (left) flows. It should be noted that high fluorescence intensities were also observed near the microchannel walls, owing to surface-adsorbed dye. For clarity, these regions were excluded from the plots. Fluorescence owing to the scanning swing-back loop is, however, still observed.

focal multiphoton microscope (TriMScope, LaVision Biotec, Bielefeld, Germany) coupled to an ultrafast time-gated intensified camera (HRI, Kentech Instruments, Didcot, UK), which is described in detail elsewhere.[11] The two-photon fluorescence-lifetime imaging system used in this study is schematically represented in Figure 1. The time-gated intensifier allows 500-ps time-gated images to be acquired at different delays after excitation, thereby sampling the fluorescence-decay profiles. For polarization resolution, a two-channel imager (PRI; DualView, Optical Insights Inc, Tucson, AZ) splits the image into two subimages resolved with orthogonal polarizations that can then be overlaid to calculate the fluorescence anisotropy. Time-gated fluorescence-intensity and -anisotropy data are then analyzed by using home-developed MatLab (The Mathworks, Natick, MA) routines.

A low-Reynolds-number poly(dimethylsiloxane) (PDMS) molded microfluidic device was fabricated.[11] The microchip layout comprises two inlets, a 50-μm-wide, 60-μm-deep, and 7-cm-long mixing channel, and a common outlet. To study DNA–dye binding within the microfluidic system, purified 5.8-kbp DNA plasmids (200 μM, 45% AT content) and aqueous solutions of H33258 (15 μM) were hydrodynamically introduced through the two inlet channels at volumetric flow rates of 50 and 100 nL min$^{-1}$, respectively. For the current device under normal operating conditions, flow is laminar (with a Reynolds number of 0.03) and mixing between component streams occurs by diffusion only. This is evident from the time-integrated fluorescence-intensity images of a $45 \times 50$ μm section of the microchannel presented in Figure 2.

At short residence times (Figure 2a) close to the point of confluence, a sharp increase in the time-integrated fluorescence intensity is observed as the H33258 molecules bind DNA plasmids in the locality of the flow interface between the two streams. With increasing residence time (Figure 2b), the fluorescence intensity increases asymmetrically across the channel, with a bias towards the DNA flow side since the smaller H33258 molecules diffuse more rapidly into the DNA flow than vice versa. At long residence times, when mixing is complete, a symmetric fluorescence-intensity profile is observed across the channel, as expected (Figure 2c). It should be noted that in some cases a significant increase in fluorescence intensity is also observed in the locality of the microchannel walls. We attribute this observation to non-specifically adsorbed, immobilized H33258 molecules (data not shown). By using two-photon excitation, however, we could selectively excite fluorescence in a single optical plane and thus minimize the contribution of any surface effects on our flow-interface measurements.

Time-gated fluorescence measurements were subsequently performed across the microchannel (with a spatial resolution of 1 μm), at residence times equivalent to those in the data presented in Figure 2. All data were analyzed globally by using a biexponential decay function, where the recovered decay times are common to all data sets. Fits for all data sets are of good quality and clearly demonstrate the existence of two discrete molecular populations, one with a characteristic decay time of 300 ps (indicative of free H33258 molecules) and one with a characteristic decay time of approximately 3500 ps (indicative of the formation of specific complexes between H33258 and DNA). Although detailed analysis has shown that H33258 molecules can interact with DNA through several binding modes, a two-state model is

  

considered to be a reasonable approximation at the relatively low H33258/base-pair ratio used in the current studies.[14] Figure 3a displays false-color-scale images of the mean fluorescence-decay time, obtained at equivalent residence times to those of the images displayed in Figure 2. A marked

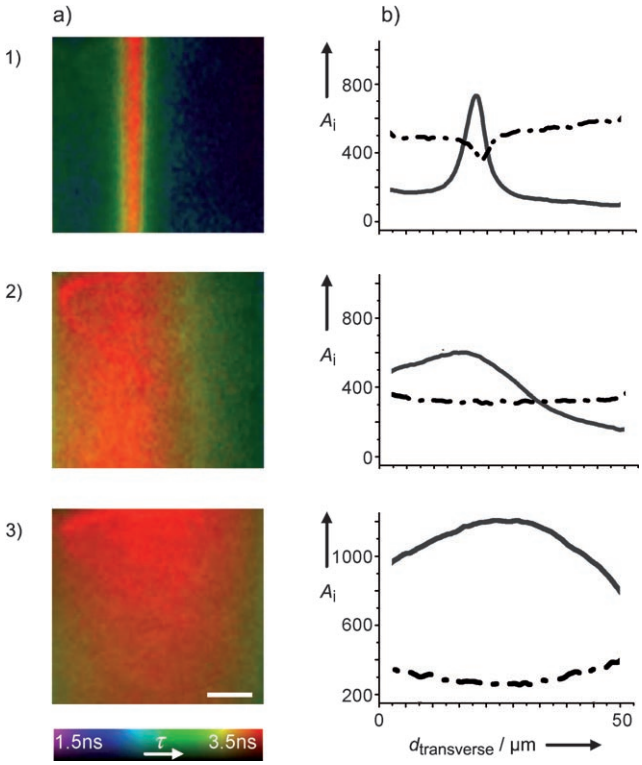


***Figure 3.*** Representative data of time-resolved fluorescence imaging at equivalent residence times to those for Figure 2: 1) $t = 300$ ms, 2) $t = 7.2$ s, 3) $t \rightarrow \infty$. a) False-color-scale maps of the mean fluorescence-decay time. The scale bar represents 10 µm. b) Recovered preexponential factors ($A_i$) from global analysis of fluorescence decays for a biexponential decay model with component lifetimes of 300 ps and 3.5 ns. The distribution of the long-lifetime component (solid line) corresponds to DNA-bound H33258 and the distribution of the short-lifetime component (dot–dash line) corresponds to unbound H33258. The third profile (b) is plotted on an offset scale to account for the increase in fluorescence at residence time $t \rightarrow \infty$.

increase in the mean fluorescence lifetime is observed in the regions of interdiffusion between the two flows where the H33258 fluorophore forms a stably bound complex with the DNA. Further information can, however, be obtained by resolving the multiple components of the fluorescence decay.

Figure 3b displays profiles of the amplitude of each decay component across the channel at various residence times. Visual inspection shows that the spatial variation of the amplitude of the component with a long (3.5 ns) decay time at all residence times demonstrates close correspondence with the variation in time-integrated fluorescence intensities (Figure 2) and therefore provides a useful diagnostic indicator of the progress of mixing. A short-lifetime (300 ps) component is also isolated. Initially the corresponding preexponential factor is greater in the H33258 flow (Figure 3b, first profile), but it subsequently becomes uniform across the channel (Figure 3b, second profile). At the end point, this preexponential factor decreases throughout the channel. This behavior corresponds to free H33258 molecules diffusing throughout the DNA flow and then being depleted as they bind to DNA. At a residence time of 7.2 s, the mean interdiffusion distance of free H33258 molecules in aqueous solution is approximately 46 µm (based on a diffusion coefficient of $D \approx 300\ \mu m\, s^{-2}$), which results in nearly complete diffusion across the 50 µm wide channel, as observed in Figure 3b, second profile.

By taking the amplitude of the preexponential factors ($A_i$) to be proportional to the populations of free and bound H33258, the relative population of the unbound fraction in the region of mixing can be estimated to be as much as ≈30% at a residence time of 7.2 s; this value decreases to less than 10% as $t \rightarrow \infty$. This analysis, directly facilitated by the ability to rapidly extract time-resolved fluorescence images from the system, thus allows resolution and relative quantification of multiple states of the H33258 molecules. This is ultimately limited by the temporal resolution of the system of ≈100 ps, which is sufficient for resolution of the population of free H33258. By comparison, time-integrated fluorescence measurements are unable to discriminate between binding events and changes in local dye concentration or variations in experimental conditions and thus can only provide qualitative information about DNA–dye interactions.

To further characterize the DNA–H33258 binding interactions, time-resolved, fluorescence-anisotropy measurements were performed to probe the rotational mobility of free and bound H33258. Figure 4 displays both time-averaged and time-resolved fluorescence-anisotropy data for equivalent residence times to those of the profiles shown in Figures 2 and 3. Figures 4a and 2a–c, bottom show close correspondence, with areas of high fluorescence anisotropy being equivalent to areas of high fluorescence intensity. Anisotropy provides a direct diagnostic indicator of DNA–dye interactions and mixing since binding restricts the rotational mobility of the dye molecules and yields increased anisotropy values.

Time-gated fluorescence-anisotropy data were analyzed by using a biexponential decay model corresponding to a two-state model of binding. In Figure 4b, an approximately 10-ns-long rotational correlation with a preexponential-factor profile matching that of the time-integrated fluorescence anisotropy and intensity is observed. Interestingly, the correlation time is lower than expected for the rotational motion of a 5.8-kpb plasmid. This observation is likely to be due to torsional motion of DNA plasmids or rotation of H33258 molecules in their binding state. A component with a short (≈500 ps) correlation time is also isolated, with a preexponential-factor profile representing the diffusion of free H33258 molecules. From the Stokes–Einstein–Debye relation, the short correlation time is consistent with the rotational motion of free H33258 molecules and reflects a mean molecular radius of 0.72 nm. From both the time- and polarization-resolved data, isotropic-fluorescence-decay data can be reconstructed that are equivalent to those in Figure 3, albeit here with reduced temporal resolution.

Observation of both the fluorescence lifetime and the rotational correlation time at various residence times after the

  

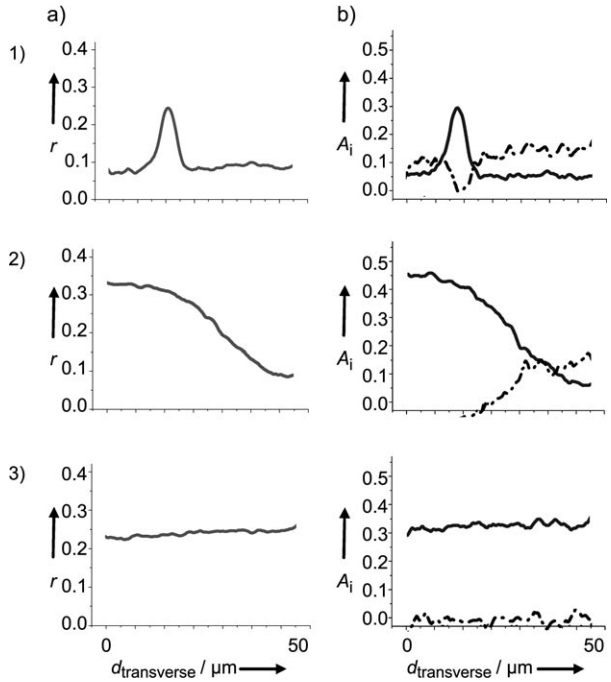


***Figure 4.*** Representative data from time-resolved fluorescence-anisotropy imaging at equivalent residence times to those for Figure 2: 1) $t = 300$ ms, 2) $t = 7.2$ s, 3) $t \rightarrow \infty$. a) Steady-state fluorescence-anisotropy profiles across the microchannel. Regions of high fluorescence anisotropy correspond to reduced rotational mobility due to binding of H33258. b) Recovered preexponential factors ($A_i$) from global analysis of fluorescence-anisotropy decays for a biexponential decay model with time constants of 500 ps and 10 ns. The distribution of the long-lifetime component (solid line) again corresponds to DNA-bound H33258 and the distribution of the short-lifetime component (dash–dot line) corresponds to unbound H33258.

initiation of mixing allows the resolution of multiple fluorescing states, which is particularly advantageous in the resolution of complicated reaction mechanisms. In the current studies, at short residence times (0.3 s and 7.2 s) a population of unbound H33258 molecules was resolved in regions of mixing and could be compared with an absence of this population at the end-point state (with stationary-flow conditions). This indicates that these short-residence-time states are far from equilibrium conditions. By using the analysis presented by Salmon et al.,[15] where reaction–diffusion–reaction times are considered, it may also be possible to quantify the kinetics of such interactions. This approach is conceptually similar to studies presented by Lipman et al.,[16] where protein-folding and -unfolding transitions were probed with single-molecule fluorescence-resonance energy-transfer (FRET) analysis, thereby allowing subpopulations to be resolved in nonequilibrium states. In the studies described herein, however, ensemble-based detection facilitates the resolution of multiple interaction states.

Microfluidic DNA-hybridization studies, such as those reported by Heule and Manz,[17] have until now been limited in their ability to discriminate intercalated dye from unbound dye or, more importantly, from dye intercalating into dimerized single-stranded DNA. The use of fluorescence-lifetime imaging in such applications would provide a direct route to both species discrimination and population quantification.

Significantly, the ability to image fluorescence parameters such as lifetime, spectrum, and polarization in three dimensions at high spatial resolution dramatically expands the information content accessible for a chemical or biological system. It should be appreciated that, although microfluidic systems afford precise control over experimental parameters such as reagent concentration and temperature,[18] extraction of the generated information is normally inefficient. The application of the fluorescence-lifetime imaging modalities described herein dramatically expands the information that can be extracted from such systems.

To summarize, the implementation of quantitative time-resolved fluorescence-imaging techniques provides a powerful route to the resolution and quantification of multistate chemical and biological systems. In conjunction with microfluidic technology affording precise spatial and temporal reaction control, as well as high signal integration, this is a powerful technique, applicable to a wide range of studies.

Received: October 6, 2006
Published online: January 23, 2007

**Keywords:** fluorescence · imaging · intercalation · microfluidics · microreactors

[1] P. S. Dittrich, K. Tachikawa, A. Manz, *Anal. Chem.* **2006**, *78*, 3887 – 3908.
[2] A. J. de Mello, *Nature* **2006**, *442*, 394 – 402.
[3] M. U. Kopp, A. J. de Mello, A. Manz, *Science* **1998**, *280*, 1046 – 1048.
[4] P. S. Dittrich, A. Manz, *Nat. Rev. Drug Discovery* **2006**, *5*, 210 – 218.
[5] J. Pihl, J. Sinclair, E. Sahlin, M. Karlsson, F. Petterson, J. Olofsson, O. Orwar, *Anal. Chem.* **2005**, *77*, 3897 – 3903.
[6] L. Cai, N. Friedman, X. S. Xie, *Nature* **2006**, *440*, 358 – 362.
[7] P. Yager, T. Edwards, E. Fu, K. Helton, K. Nelson, M. R. Tam, B. H. Weigl, *Nature* **2006**, *442*, 412 – 418.
[8] M. A. Schwarz, P. C. Hauser, *Lab Chip* **2001**, *1*, 1 – 6.
[9] J. Siegel, D. S. Elson, S. E. D. Webb, D. Parsons-Karavassilis, S. Leveque-Fort, M. J. Cole, M. J. Lever, P. M. W. French, M. A. A. Neil, R. Juskaitis, L. O. Sucharov, T. Wilson, *Opt. Lett.* **2001**, *26*, 1338 – 1340.
[10] R. K. P. Benninger, Y. Koç, O. Hofmann, J. Requejo-Isidro, M. A. A. Neil, P. M. W. French, A. J. de Mello, *Anal. Chem.* **2006**, *78*, 2272 – 2278.
[11] R. K. P. Benninger, O. Hofmann, J. McGinty, J. Requejo-Isidro, I. Munro, M. A. A. Neil, A. J de Mello, P. M. W. French, *Opt. Express* **2005**, *13*, 6275 – 6285.
[12] S. W. Magennis, E. M. Graham, A. C. Jones, *Angew. Chem.* **2005**, *117*, 6670 – 6674; *Angew. Chem. Int. Ed.* **2005**, *44*, 6512 – 6516.
[13] *Principles of Fluorescence Spectroscopy* (Ed.: J. R. Lackowicz), Plenum, New York, **2006**.
[14] S. Y. Breusegem, F. G. Loontiens, P. Regenfuss, R. M. Clegg, *Drug–Nucleic Acid Interact.* **2001**, *340*, 212 – 233.
[15] J. B. Salmon, C. Dubrocq, P. Tabeling, S. Charier, D. Alcor, L. Jullien, F. Ferrage, *Anal. Chem.* **2005**, *77*, 3417 – 3424.
[16] E. A. Lipman, B. Schuler, O. Bakajin, W. A. Eaton, *Science* **2003**, *301*, 1233 – 1235.
[17] M. Heule, A. Manz, *Lab Chip* **2004**, *4*, 506 – 511.
[18] S. K. W. Dertinger, D. T. Chiu, N. L. Jeon, G. M. Whitesides, *Anal. Chem.* **2001**, *73*, 1240 – 1246.

  